

Microgrid Day-Ahead Scheduling Considering Neural Network based Battery Degradation Model

Cunzhi Zhao, *Student Member, IEEE* and Xingpeng Li, *Senior Member, IEEE*

Abstract— Battery energy storage system (BESS) can effectively mitigate the uncertainty of variable renewable generation. Degradation is unpreventable for batteries such as the most popular Lithium-ion battery (LiB). The main causes of LiB degradation are loss of Li-ions, loss of electrolyte, and increase of internal resistance which are hard to model and predict. In this paper, we propose a data driven method to predict the battery degradation per a given scheduled battery operational profile. Particularly, a neural network based battery degradation (NNBD) model is proposed to quantify the battery degradation with inputs of major battery degradation factors. When incorporating the proposed NNBD model into microgrid day-ahead scheduling (MDS), we can establish a battery degradation based MDS (BDMDS) model that can consider the equivalent battery degradation cost precisely. Since the proposed NNBD model is highly non-linear and non-convex, BDMDS would be very hard to solve. To address this issue, a neural network and optimization decoupled heuristic (NNODH) algorithm is proposed in this paper to effectively solve this neural network embedded optimization problem. Simulation results demonstrate that the proposed NNODH algorithm is able to obtain the optimal solution with lowest total cost including normal operation cost and battery degradation cost.

Index Terms— Battery degradation, Battery energy storage system, Energy management system, Machine learning, Microgrid day-ahead scheduling, Neural network, Optimization.

NOMENCLATURE

Sets:

S_T	Set of time intervals.
S_G	Set of controllable micro generators.
S_S	Set of energy storage systems.
S_{WT}	Set of wind turbines.
S_{PV}	Set of PV systems.

Parameters:

c_{Gi}	Linear cost for controllable unit i .
c_{Gi}^{NL}	No load cost for controllable unit i .
c_{Gi}^{SU}	Start-up cost for controllable unit i .
ΔT	Length of a single dispatch interval.
R_{prcent}	Percentage of the backup power to the total power.
E_{Si}^{Max}	Maximum energy capacity of ESS i .
E_{Si}^{min}	Minimum energy capacity of ESS i .
U_{Buy}^t	Status of buying power from main grid in time interval t .
U_{Sell}^t	Status of selling power to main grid status in time t .
c_{Buy}^t	Wholesale electricity purchase price in time interval t .
c_{Sell}^t	Wholesale electricity sell price in time interval t .
P_{Gi}^{Max}	Maximum capacity of generator i .

Cunzhi Zhao and Xingpeng Li are with the Department of Electrical and Computer Engineering, University of Houston, Houston, TX, 77204, USA (e-mail: czhao20@uh.edu; Xingpeng.Li@asu.edu).

P_{Gi}^{Min}	Minimum capacity of generator i .
P_{Gi}^t	Output of generator i in time interval t .
$U_{Char}^{t,i}$	Charging status of energy storage system i in time interval t . It is 1 if charging status; otherwise 0.
$U_{Disc}^{t,i}$	Discharging status of energy storage system i in time interval t . It is 1 if discharging status; otherwise 0.
U_G^{ti}	Status of generator i in time interval t . It is 1 if on status; otherwise 0.
V_G^{ti}	Startup indicator of Status of generator i in time interval t . It is 1 if unit i starts up; otherwise 0.
P_{Buy}^t	Amount of power purchased from main grid power in time interval t .
P_{Sell}^t	Amount of power sold to main grid power in time interval t .
P_L^t	Demand in the microgrid in time interval t .
$P_{Disc}^{t,i}$	Discharging power of energy storage system i at time t .
$P_{Char}^{t,i}$	Charging power of energy storage system i at time t .
P_{Max}^{Grid}	Maximum thermal limit of tie-line between main grid and microgrid.
P_{Gi}^{Ramp}	Ramping limit of diesel generator i .
P_{Si}^{Max}	Maximum charge/discharge power of BESS i .
P_{Si}^{Min}	Minimum charge/discharge power of BESS i .
η_{Si}^{Disc}	Discharge efficiency of BESS i .
η_{Si}^{Char}	Charge efficiency of BESS i .

I. INTRODUCTION

Renewable energy sources (RES) will play an important role in future microgrid due to the 3-D (decentralization, decarbonation, and digitalization) trend. The proportion of RES in power generation is growing significantly. However, the system stability is substantially weakened by the stochastic and intermittent generation of high penetration RES. Battery energy storage system (BESS) is an effective flexible solution for addressing the uncertainty of variable RES induced system. The high cost of battery in the past decade limits the deployment of BESS that leads to a limited capacity of installed BESS [1]. However, the unit price of BESS keeps decreasing and is predicted to be 80% lower in the next five years. Thus, much more BESSs will be available in bulk power systems and small-scale microgrids in near future.

The characteristic of rechargeable battery makes it degrade during cycling and leads to calendar aging when it is idle. This degradation can be accelerated by extreme fast charging or discharging schedules, extreme low or high ambient temperature and overcharging or over discharging. The internal states of battery remain difficult to estimate while the battery is taking a more important role as BESS in power energy systems [2]. It is quite hard to predict the battery degradation. The

working principle of a BESS is similar to a voltage source in series with impedances. However, the operating conditions and environments are various for BESS in microgrids, as well as in bulk power systems. Thus, the BESS model cannot be simply treated as a voltage-source based model [3]. The main component of BESS is battery. Li-ion battery (LiB) has been widely used as energy storage due to its high energy density and low memory effect nature. In the view of chemical layer, lithium-ions move from the negative electrode through an electrolyte to the positive electrode when LiB is discharging and move from the positive electrode through an electrolyte to the negative electrode when LiB is charging. LiB degrades mainly because of the loss of Li-ions, the loss of electrolyte and the increase of internal resistance. During battery cycling, the influential factors that cause the degradation include the battery operating ambient temperature, charging/discharging rate, state of charge (SOC), state of health (SOH), and depth of discharge (DOD) [4]-[5].

Previous studies have well researched on energy management strategies of BESS-integrated microgrids. In [6]-[13], it has been proved that the BESS can be seamlessly integrated into microgrid especially for those microgrids with high penetration renewable energy sources. However, they did not consider the effect of battery degradation. In [14], DOD is used to calculate the remaining useful cycle. The battery degradation is estimated based on the remaining useful battery cycle and the actual capacity. The only variable considered in [14] is the DOD and they assume the degradation process to be linear throughout the battery life which is not reasonable. Pascali in [15] adopts the Butler-Volmer equation for battery degradation model to illustrate the diffusion of the solvent reactants. However, the data are based on the experiment for different discharge currents and SOC values, which are not sufficient as they omit other important factors contributing to battery degradation. A battery degradation assessment framework is proposed with a degradation coefficient to represent the linear approximation of battery degradation in a short period of time in [16]. As mentioned in [16], the linear assumption of battery degradation may simplify the problem and reduce the computational difficulty, but the degradation value may not be accurately predicted. Similarly, in [17]-[19], a linear degradation rate is used to quantify battery degradation and calculate the equivalent degradation cost. Saldana's paper [20] proposed a battery degradation matrix reference for electric vehicle (EV). However, it is hard to consider this model in the microgrid day-ahead scheduling (MDS). The electric vehicle has been researched and conducted in the V2G system in [21]-[23] due to the similarity between EV and BESS. However, a very important EV battery degradation factor, the charge/discharge rate, is neglected in those papers. A data driven degradation model is presented in [24]. A quadratic equation is formed based on the collected data. The data are collected only under different profiles of DOD and SOC. This indicates the lack of other critical degradation factors is the weakness for this model. For all the aforementioned battery degradation models, they ignore several critical degradation factors, which limits accuracy of the battery degradation prediction; none of them provides a comprehensive model to cover all critical degradation factors; moreover, some of the degradation models are too complex to be incorporated with MDS.

To address the gap mentioned above, a fully connected neural network (NN) is proposed to train a battery degradation model and accurately predict the battery degradation. The input of the neural network is a vector of five variables including ambient temperature, charging/discharging rate, SOC, DOD and SOH. This neural network based battery degradation (NNBD) model is very complex since it is highly non-linear and non-convex. When incorporating the proposed NNBD model into MDS, we can establish a battery degradation based MDS (BDMDS) model that can consider the equivalent battery degradation cost precisely. However, such a complex neural network embedded optimization problem would be hard to solve directly. To address this issue, a neural network and optimization decoupled heuristic (NNODH) algorithm is proposed in this paper to effectively solve the BDMDS problem. The proposed NNODH algorithm iteratively solves the transformed BDMDS problem that is decoupled to the battery degradation calculation and MDS optimization problems. Additional BESS operation constraints with tighter bounds will be generated in each iteration to limit the usage of BESS which can reduce the battery degradation and relevant cost in the next iteration. However, the microgrid operation cost will increase if the BESS usage is limited. The goal of the proposed NNODH algorithm is to find the lowest value for the sum of battery degradation cost and microgrid operation cost. It can also record the total cost for each iteration and locate the vertex point which is also the optimal solution for the BDMDS problem.

The main contributions of this paper are presented as follows:

- A set of battery cycle generators is designed to simulate battery degradation under different battery operational profiles. Four features (ambient temperature, discharge rate, SOC level, and DOD) that affect battery degradation are collected, along with the updated battery energy capacity for each cycle.
- A neural network based battery degradation model with five input features (SOH level, ambient temperature, charging/discharging rate, SOC level, and DOD) is proposed in this paper and it is able to accurately predict the degradation percentage respect to the original capacity.
- A BDMDS model is proposed to capture the effect of battery degradation by incorporating the proposed NNBD model in microgrid energy management.
- An NNODH algorithm is proposed to efficiently solve and provide the optimal solution for the BDMDS model that is hard to solve directly. Four conserved MDS models that include different constraints to limit the BESS usage are developed. The optimal scheduling obtained with NNODH leads to the lowest total cost including the battery degradation cost and microgrid operation cost.
- Validation of the performance for the proposed NNODH algorithm is conducted. Case studies prove that by limiting the battery operation that leads to lower degradation, the total cost can be reduced significantly.

The rest of the paper is organized as follows. Section II presents a traditional MDS model. Section III presents the neural network structure of the proposed battery degradation model and Section IV presents the proposed microgrid energy management strategies with the BESS degradation model. Section

V discusses the microgrid testbed, simulation results and sensitivity analysis. Section VI concludes the paper.

II. TRADITIONAL MICROGRID DAY-AHEAD SCHEDULING

A traditional MDS model is established as a benchmark model to gauge the proposed BDMDS model. This traditional MDS model consists of (1)-(15) as described below and it does not consider battery degradation.

The objective of this traditional MDS model is to minimize the total cost of the microgrid operations as illustrated in (1). The power balance equation involving controllable generators, renewable energy sources, power exchange with the main grid, BESS output and the load is shown in (2). Constraint (3) enforces the power limits of the controllable units such as diesel generators. The ramping up and down limits are enforced by (4) and (5). Equation (6) ensures the status of power exchange between microgrid and main grid to be either purchasing or selling or be idle. The thermal limit of the tie-line is enforced by constraints (7)-(8). Equation (9) restricts the BESS to be either in charging mode or in discharging mode or stay idle. Constraints (10)-(11) limit the charging/discharging power of BESS. As shown in (12), the SOC level of BESS can be calculated based on current energy stored in BESS. Equation (13) calculates the energy stored in the BESS for each time interval. The ending BESS SOC level is forced to equal to the initial value (14). Constraint (15) ensures the microgrid to have sufficient backup power to address some outage events.

Objective:

$$f^{MG} = \sum \sum (P_{Gi}^t c_{Gi} + U_{Gi} c_{Gi}^{NL} + V_{Gi} c_{Gi}^{SU}) + P_{Buy}^t c_{Buy}^t - P_{Sell}^t c_{Sell}^t \quad (i \in S_G, t \in S_T) \quad (1)$$

Constraints are as follows:

$$P_{Buy}^t + \sum_{i \in S_G} P_{Gi}^t + \sum_{i \in S_{WT}} P_{WTi}^t + \sum_{i \in S_{PV}} P_{PVi}^t + \sum_{i \in S_S} P_{Disc}^t = P_{Sell}^t + \sum_{i \in S_L} P_{Li}^t + \sum_{i \in S_S} P_{Char}^t \quad (2)$$

$$P_{Gi}^{Min} \leq P_{Gi}^t \leq P_{Gi}^{Max} \quad (i \in S_G, t \in S_T) \quad (3)$$

$$P_{Gi}^{t+1} - P_{Gi}^t \leq \Delta T \cdot P_{Gi}^{Ramp} \quad (i \in S_G, t \in S_T) \quad (4)$$

$$P_{Gi}^t - P_{Gi}^{t+1} \leq \Delta T \cdot P_{Gi}^{Ramp} \quad (i \in S_G, t \in S_T) \quad (5)$$

$$U_{Buy}^t + U_{Sell}^t \leq 1 \quad (i \in S_G, t \in S_T) \quad (6)$$

$$0 \leq P_{Buy}^t \leq U_{Buy}^t \cdot P_{Grid}^{Max} \quad (t \in S_T) \quad (7)$$

$$0 \leq P_{Sell}^t \leq U_{Sell}^t \cdot P_{Grid}^{Max} \quad (t \in S_T) \quad (8)$$

$$U_{Disc}^t + U_{Char}^t \leq 1 \quad (i \in S_G, t \in S_T) \quad (9)$$

$$U_{Char}^t \cdot P_{Si}^{Min} \leq P_{Char}^t \leq U_{Char}^t \cdot P_{Si}^{Max} \quad (i \in S_S, t \in S_T) \quad (10)$$

$$U_{Disc}^t \cdot P_{Si}^{Min} \leq P_{Disc}^t \leq U_{Disc}^t \cdot P_{Si}^{Max} \quad (i \in S_S, t \in S_T) \quad (11)$$

$$SOC_{Si}^t = E_{Si}^t / E_{Si}^{Max} \quad (i \in S_S, t \in S_T) \quad (12)$$

$$E_{Si}^t - E_{Si}^{t-1} + \Delta T \cdot (P_{Disc}^{t-1,i} / \eta_{Si}^{Disc} - P_{Char}^{t-1,i} \eta_{Si}^{Char}) = 0 \quad (i \in S_G, t \in S_T) \quad (13)$$

$$E_{Si}^{t=24} = E_{Si}^{Initial} \quad (i \in S_S) \quad (14)$$

$$P_{Grid}^{Max} - P_{Buy}^t + P_{Sell}^t + \sum_{i \in S_G} (P_{Gi}^{Max} - P_{Gi}^t) \geq R_{percent} (\sum_{i \in S_L} P_{Li}^t) \quad (t \in S_T) \quad (15)$$

III. NEURAL NETWORK BASED BATTERY DEGRADATION MODELING

The traditional microgrid day-ahead scheduling model determines the optimal operational profiles for BESS, controllable generators and tie-line exchange power. However, the BESS in the traditional MDS model is considered to be ideal

without any degradation and the equivalent cost of battery degradation is zero. This may substantially accelerate the aging and replacement of expensive BESS which may lead to economic loss in the long run. Besides, the BESS degradation needs to be accurately quantified for various battery daily operational profiles to obtain the truly optimal scheduling solutions. Thus, a deep learning method, particularly a deep neural network, is proposed in this section to accurately predict the BESS degradation.

A. Input Data

The deep neural network method is applied to learn and predict the battery degradation based on several critical features. A battery model implemented in the MATLAB Simulink [25] is used to conduct the battery aging tests. This battery model can simulate various types and configurations of batteries, various conditions, and operating profiles. Built upon this battery model, a battery cycle generator is designed to simulate the charging and discharging cycles under preset charging/discharging rates. For each battery aging test, each cycle is simulated to discharge from a certain SOC to a certain lower SOC and then charge back to the starting SOC. The data collected from the simulations include four input variables: ambient temperature, charging/discharging rate, SOC, and DOD. The battery's energy capacity level for each cycle is also collected for the calculation of each cycle's battery degradation value. Table I shows the numbers of battery aging tests that are simulated under different SOC and DOD. Each battery aging test represents a group of simulated battery profile under initial SOC and fixed DOD until the battery capacity degrades to 80% of the maximum rated capacity. For instance, the "4" in Table I means there are four battery aging tests that are simulated at an initial SOC level of 100% with a DOD level of 10%. In other words, for a single cycle of the simulation, the battery will discharge from 100% to 90% SOC and then charge back from 90% to 100% SOC. However, 100% SOC may not represent the original maximum capacity level. It depends on the SOH level. Moreover, each of these SOC&DOD combinations will be simulated multiple times under different ambient temperatures and charging/discharging rates. The charging/discharging rate is also referred as C rate. As is shown in (16), C rate describes how fast the battery can be charged from empty to full capacity or be fully discharged from the maximum capacity to empty. For example, 2C means the battery will discharge the 100% full capacity in 0.5 hour.

$$C \text{ rate} = \frac{I_{Battery}}{E_0} \quad (16)$$

where $I_{Battery}$ represents the charging/discharging current of the BESS and E_0 denotes the original battery rated capacity.

Note that the C rate is constant in the simulation for each SOC&DOD combination, which means that the time for single discharge cycle varies with different DOD levels. Fig. 1 shows the distribution of numbers of battery aging tests with different C rates. The total number of the battery aging tests that are simulated with different values of degradation factors is 945. For each battery aging test, it contains the battery capacity data for each cycle until the capacity reaches to 80% of the maximum rated capacity that is considered the end of a battery's life. This indicates each battery aging test may contain different numbers of cycles. It is common to consider the 80%

of the rated capacity as the end of battery's life in battery aging test [26]. Fig. 2 shows the SOH curves of 50 randomly selected battery aging tests. The x-axis is the cycle number, and the last cycle represents the cycle that the battery reaches the 80% of its maximum rated capacity.

TABLE I Numbers of battery aging tests under various SOC and DOD levels

	Initial SOC	100 %	80 %	60 %	50 %	40 %	20 %
DOD (%)	20%	4	5	17	23	22	23
	30%	20	34	36	32	37	/
	40%	36	41	41	40	44	/
	50%	38	41	36	42	/	/
	60%	37	37	37	/	/	/
	70%	41	36	/	/	/	/
	80%	39	35	/	/	/	/
	90%	35	/	/	/	/	/
	100%	36	/	/	/	/	/

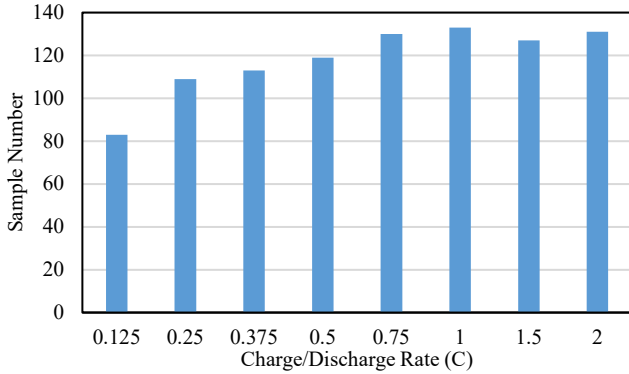


Fig. 1. Density distribution of battery aging tests per charge/discharge rate.

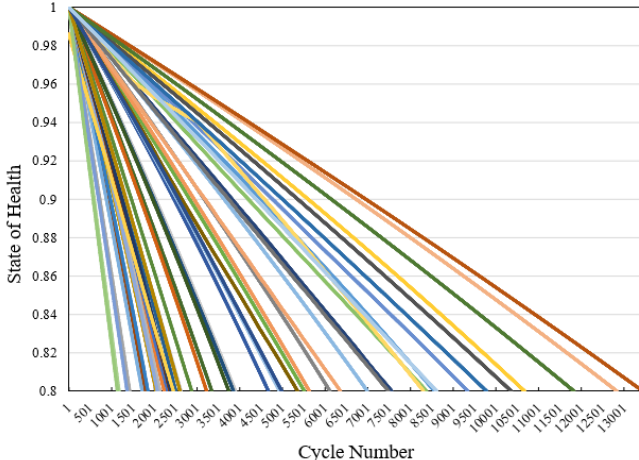


Fig. 2. Simulated results for a subset of battery aging tests.

B. Data Pre-processing

The battery capacity level in percent or SOH at the end of each cycle is recorded from each battery aging test simulation. Battery degradation per cycle is defined as the difference between the initial SOH and ending SOH for a given cycle. However, for some battery aging tests with low C rates and small DODs, the degradation for some cycles may be too less to measure and could even be zero. Also, some of the degradation data contain outlier points which may require some further process for a better training result. The battery degradation data are processed with different methods: (i) raw, (ii) smoothed method, and (iii) regressed method, are as shown in

Fig. 3. “Raw” represents the original data without any pre-processing and the associated training results can be considered as a benchmark to gauge the effectiveness of the other two proposed pre-processing methods. The smoothed method filters out the outliers of the original data. Regressed method applies linear regression on the smoothed data. The data after being processed by the three methods will be fed into the NN separately to evaluate their performance. Also, all three groups of input data are normalized to increase the training efficiency. The normalization used in [27] is applied in the data pre-processing and shown in (17). The expectation and variance are computed over training dataset for each input variable. At last, the input data will be split into two parts, 80% as the training dataset and 20% as the validation dataset.

$$\widehat{x}_k = \frac{x_k - E(x_k)}{\sqrt{Var(x_k)}} \quad (17)$$

where $E(x_k)$ represents the expectation of x_k and $Var(x_k)$ represents the variance of the x_k .

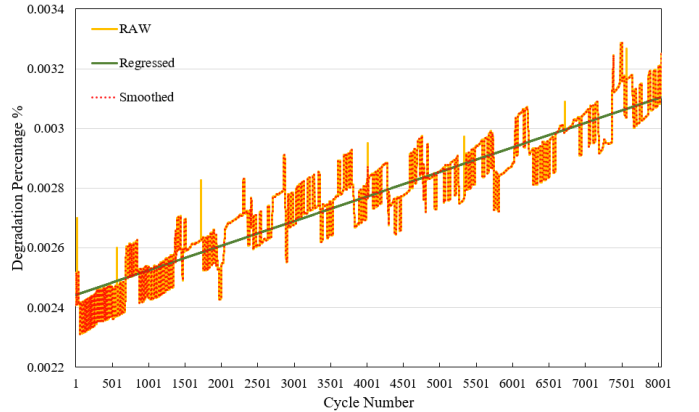


Fig. 3. Battery degradation data under different data processing methods.

C. The Proposed NNBD Model

A fully connected neural network is constructed to model the battery degradation. Five aging factors (ambient temperature, C rate, SOC, DOD and SOH) form a five-element input vector for the neural network. Each input vector corresponds with a single output value which is the amount of battery degradation in percentage respect to the SOH level for the same cycle. A dynamic learning rate scheme is used in the training process to improve the training result. The learning rate will decrease automatically after a certain amount of training epochs. The structure of the trained neural network is shown in Fig. 4 plotted by NN-SVG [28]. It has an input layer with 5 neurons, first hidden layer with 20 neurons, second hidden layer with 10 neurons and an output layer with 1 neuron.

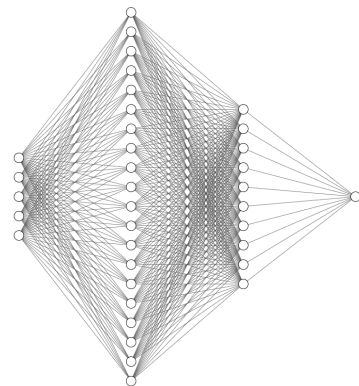


Fig. 4 Structure of the proposed neural network model for battery degradation.

The mini batch gradient descent strategy is applied to train the neural network. Different batch sizes are tested to achieve the best training results. As defined in (18), mean squared error (MSE) represents the average of the square of the difference between the actual and predicted values over all training data points. MSE is used as the criterion, a loss function, to train the neural network and measure the neural network quality.

$$MSE = \frac{1}{n} \sum_{i=1}^n (y_i - \tilde{y}_i)^2 \quad (18)$$

D. Incorporating NNBD into Microgrid Scheduling

When considering battery degradation in microgrid day-ahead scheduling, the objective function needs to be updated by including the associated equivalent battery degradation cost. The updated objective function is as follows,

$$f = f^{MG} + f^{BESS} \quad (19)$$

where f^{MG} is defined in (1); and f^{BESS} denotes the battery degradation cost that can be estimated by the proposed NNBD model. f^{BESS} can be calculated as follows.

$$f^{BESS} = c_{BESS}^{Capital} \sum_t NN(T, C, SOC, DOD, SOH) \quad (20)$$

where $c_{BESS}^{Capital}$ represents the capital investment cost of BESS; T and C represent the ambient temperature and C rate respectively.

Thus, the proposed BDMDS model can be represented by (2)-(15) and (19)-(20).

IV. THE PROPOSED NNODH FOR MICROGRID SCHEDULING

The proposed battery degradation based microgrid day-ahead scheduling model, which is presented in the above section, would be very hard to solve directly since the proposed NNBD model that is highly non-linear and non-convex is now a part of the proposed BDMDS model. To address this issue, a novel method, NNODH, is proposed in this paper to decouple the complex BDMDS model and solve it in four steps in an iterative manner.

- Step A is to solve the microgrid day-ahead scheduling with additional constraints by limiting BESS usage that is generated from Step D. Note that in the first iteration, there is no extra limit on BESS usage.
- Step B estimates BESS degradation with the proposed NNBD model that is trained beforehand.
- Step C determines whether the solutions meet the designed stopping criteria: stop the iteration process and report the solution if yes; otherwise, go to Step D.
- Step D updates the boundaries that limit the BESS operations to reduce the degradation cost; and the associated constraints will be sent to Step A to be included in MDS for the next iteration.

This iterative procedure is illustrated in Fig. 5.

A. Microgrid Scheduling

The traditional microgrid day-ahead scheduling that is introduced in Section II is conducted to obtain an initial solution that does not consider the battery degradation. It is solved only once in the first iteration. When considering battery usage limiting constraints that will be presented in Section IV.C, MDS would be referred to as conserved MDS (CMDS) in this paper. To sum up, traditional MDS is solved for the first iteration while CMDS is solved for all subsequent iterations.

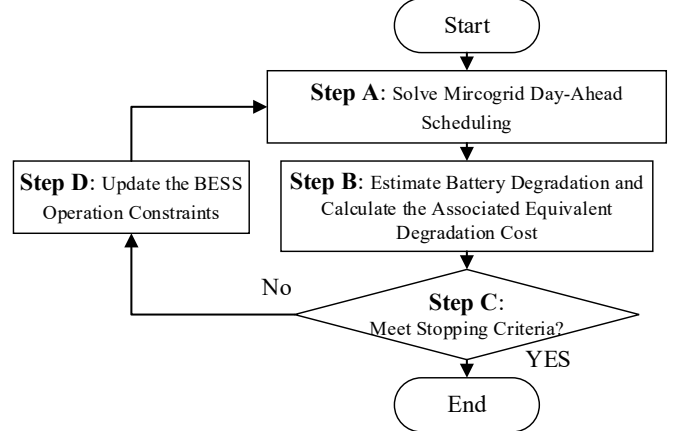


Fig. 5. Flowchart of the proposed NNODH method.

B. Battery Degradation Calculation

After solving the traditional microgrid scheduling problem in step A. The optimal solution that does not consider the battery degradation is obtained. From the solution set, SOC level are required for the input of the proposed NNBD model. The absolute value of the difference of the SOC levels between time intervals t and $t - 1$ will be the DOD level as shown in (21). C rate is calculated by (22). It is assumed that the battery SOH level is available for microgrid day ahead scheduling. The input vector can be formed as shown in (23) and then be fed into the trained neural network of battery degradation in (24). The battery degradation cost (BDC) can be calculated in (25): multiplying the battery degradation (BD) by the capital cost of the BESS.

$$DOD_t = |SOC_t - SOC_{t-1}| \quad (21)$$

$$C_t^{Rate} = DOD_t / \Delta T \quad (22)$$

$$\bar{x}_t = (T, C, SOC, DOD, SOH) \quad (23)$$

$$BD = \sum_{t \in S_T} f^{NN}(\bar{x}_t) \quad (24)$$

$$BDC = BD * c_{BESS}^{Capital} \quad (25)$$

C. Operation Limits of BESS

Since we calculate the BDC based on the BESS capital cost, a lower degradation cost indicates a longer lifetime of the BESS. After the previous iteration in steps A and B, the total cost including microgrid operation cost and the BDC are obtained. The goal of Step C is to generate extra constraints that can limit or change the battery output to reduce the battery degradation cost. The generated constraints will further tight the range that BESS can operate after each iteration. Three types of extra constraints are proposed to limit battery usage. Constraint (26) is to reduce the sum of battery output power over 24 hours by forcing it to be less than the previous iteration. We name (26) as battery consumption limit (BCL). Constraint (27) is similar to (26), but it only limits the sum of output power in top three battery output time intervals, named as precise battery consumption limit (PBCL). Constraints (28)-(29) are designed to limit the maximum charging/discharging power that is named as battery C rate limit (BRL). The proposed constraints will be generated and updated for each iteration by using the scheduled battery operational profile from previous iteration and the proposed battery operation restriction factor (BORF) α which is a preset parameter. Note that the value of BORF can determine the amount of the limits in BCL, PBCL, and BRL. Each of those three types of poten-

tial constraints will be tested separately to evaluate its performance in a microgrid testbed.

$$\sum_{t \in T} (P_{Char}^{t,i} + P_{Disc}^{t,i}) \leq (1 - \alpha) * P_{BatteryTotal}^{Pervious_SCUC} \quad (26)$$

$$\sum_{t \in Top\ 3\ Battery\ Output} P_{Disc}^{t,i} + P_{Disc}^t \leq (1 - \alpha) * P_{BatteryTotal}^{Pervious_SCUC} \quad (27)$$

$$P_{Char}^{t,i} \leq P_{Si}^{Max} (1 - \alpha)^{iteration-1} \quad (28)$$

$$P_{Disc}^{t,i} \leq P_{Si}^{Max} (1 - \alpha)^{iteration-1} \quad (29)$$

Depending on which battery usage limiting constraint is used, there are four variations of the proposed NNODH algorithm. They are all conducted to compare the performance of the proposed constraints. The detail of the proposed four variations is presented in Table II. The CMDS model in this table is solved instead of the traditional MDS model since the second iteration of the proposed NNODH algorithm.

TABLE II The proposed four NNODH strategies

Strategies	CMDS Model for Step A
NNODH-BCL	(1)-(15), (26)
NNODH-PBCL	(1)-(15), (27)
NNODH-BRL	(1)-(15), (28)-(29)
NNODH-ALL	(1)-(15), (26)-(29)

D. Iterations and Stopping Criteria

Fig. 6 illustrates the process of determining the optimal solution of BDMDS using the proposed NNODH algorithm. As is discussed in Section IV.B, the first iteration only considers the traditional microgrid day-ahead scheduling model that ignores the battery degradation. In Fig. 6, the red star denotes the global optimal solution for BDMDS that considers the proposed NNBD model; and the black star represents the solution for MDS in the current iteration while the grey star denotes the solution for the MDS problem in the previous iteration. The MDS solutions are approximations to the global optimal solution for BDMDS; they are referred to as pseudo solutions (feasible but may not be optimal) for BDMDS. Graph 1 in Fig. 6 represents the first iteration. The BESS usage limit constraints that are generated in each iteration will reduce the feasible solution area for the MDS problem in the next iteration to a smaller region. Graphs 2-4 show the feasible region shrinks for each iteration and the black star (pseudo solution) is moving towards the red star (optimal solution for BDMDS). Graph 5 shows the red star and black star overlap which indicates that the black star here is the optimal solution for the BDMDS problem. If the iteration continues, the feasible set of BDMDS will continue to reduce such that the optimal solution might be skipped. Practically, the pseudo solutions may not include the exact global optimal solution. Since the proposed NNODH algorithm is an iteration method, different BORF values used in (26)-(29) may result into different BDMDS solutions that should deviate slightly away from the global optimal solution. To ensure the best pseudo solution is close enough to the global solution with least total cost, small BORF is preferred. However, it may take more iterations for a smaller BORF to find the optimal solution.

E. Evaluation Metrics

Three metrics are designed to evaluate the performance of the proposed model: degradation cost reduction (DCR), total cost reduction (TCR) and operational cost increment (OCI). They are defined in (30), (31), and (32) respectively. The degradation cost reduction illustrates how much the BDC can be reduced as compared to the maximum value when battery deg-

radation is not considered in MDS. The TCR represents how much the total cost can be reduced by the proposed model while the OCI shows how much the operation cost would increase when considering the battery degradation model. Notations BDC^{Max} , TC^{Max} , OC^{Min} represent the maximum battery degradation cost, maximum total cost, and the minimum operation cost respectively. These parameters are obtained by solving the traditional microgrid day-ahead scheduling problem in the first iteration when battery degradation cost is not considered.

$$DCR = \frac{BDC^{Max} - BDC}{BDC^{Max}} * 100\% \quad (30)$$

$$TCR = \frac{TC^{Max} - TC}{TC^{Max}} * 100\% \quad (31)$$

$$OCI = \frac{OC - OC^{Min}}{OC^{Min}} * 100\% \quad (32)$$

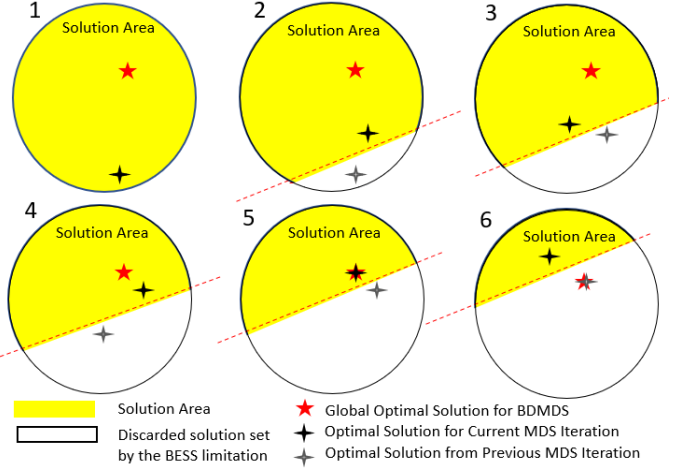


Fig. 6. Illustration of the proposed NNODH algorithm.

A stopping criterion is proposed as part of the NNODH algorithm. It is used to terminate the iterations and then the best solution can be reported. The designed stopping criteria is defined as follows: for any past 10 iterations, if the $TC^n - TC^{n-1}$ is less than 0 for the first five iterations and greater than 0 for the last five iterations, then the iteration will stop and the best solution with lowest total cost for BDMDS will be reported. Here, TC^n and TC^{n-1} denotes the total costs in n^{th} and $(n-1)^{th}$ iterations respectively. The total cost here represents the lowest total cost rather than the lowest battery degradation cost. The optimal solution will be affected by the battery size as well as the unit price.

V. CASE STUDIES

A. Microgrid Testbed

A typical grid-connected microgrid with renewable energy sources is created in this paper as a testbed to examine the proposed NNBD model, BDMDS model and NNODH algorithm. This testbed includes one 180kW diesel generator (DG), five 200kW wind turbines (WT), 300 residential houses that contains solar panel (5kW capacity per house), and a 300kWh lithium-ion based BESS with a charging/discharging efficiency of 90%. The load data representing 1000 residential houses. The ambient temperature and available solar power for a time period of 24 hours are obtained from the Pecan Street Dataport [29]. The wholesale electricity price is obtained from ECROT [30]. The price of the electricity sold to the main grid

is set to 80% of the purchase price. Sensitivity analysis is conducted with different RES penetration levels and different BESS sizes. The computer with Intel® Xeon(R) W-2295 CPU @ 3.0 GHz, 256 GB of RAM, and Nvidia Quadro RTX 8000 (48GB GPU) was utilized to conduct the numerical simulations including battery degradation model training and microgrid day-ahead resource scheduling. The microgrid resource scheduling problem studied in this work covers a total time horizon of 24 hours, which is solved using the Pyomo package [31] with the Gurobi solver [32].

B. Training Results of NNBD

The results of NNBD training and parameters tuning are presented and analyzed in this section. The parameter tuning during NN training is very important to achieve accurate and efficient training results. Mini-batch technology is used for the NN training. The optimal batch size may vary for different input data. Different training batch sizes are tested to determine the optimal training batch-size and the test results are presented in Table III. It can be observed that the batch size of 256 can achieve the highest accuracy while requiring less epochs to complete the training process. The validation accu-

racy can reach up to 94.5% while it only requires 50 epochs to reach a steady accuracy. The error tolerance is set to 15% when calculating prediction accuracy in Table III and Table IV. Larger or smaller batch size will either reduce the accuracy or increase the training epochs. We observed that large batch size can help smooth the oscillation of the training accuracy curve. The training accuracies with batch sizes of 128 and 256 are almost equally the best. However, the training accuracy curve with a batch size of 256 is much smoother than the other one. Moreover, we observed that if the input data are shuffled, then the neural network cannot obtain good results. This may be due to the characteristic of the input data: the battery degradation data are time-series data for each battery aging test. The results with different data pre-processing methods are compared in Table IV. Note that the test results in Table IV are obtained with the neural networks trained with the same batch-size of 256. The regressed data pre-processing method has the highest accuracy and efficiency. Based on the results from Table III and Table IV, the regressed method performs the best and is used for all other simulations presented below.

Table III Batch-size test

Batch-Size	16	32	64	128	256	512	1024	2048
Number of Epochs	20	20	85	110	50	50	75	75
Accuracy	40%	50%	90.5%	94.0%	94.5%	92.5%	88%	67%

Table IV Training results with different data pre-processing methods

Data Pre-processing Methods	Accuracy	Number of Epochs
Original	78%	150
Smoothed	82%	100
Regressed	94.5%	50

The best training results are shown in Fig. 7 that illustrates the training loss versus validation loss and the accuracy curves under different error thresholds. The accuracy is around 60% under a 5% error tolerance, 80% under a 10% error tolerance and 94.5% under a 15% error tolerance. The accuracy with 20% error tolerance is 95.5% which is only 1% higher than the 15% error tolerance. Thus, we choose 15% as the error tolerance level when calculating accuracy in all subsequent results. After 50 epochs, the training loss and the validation loss stop decreasing and the training accuracy becomes stable as well. The final training result stops at 65th epoch to avoid overfitting and oscillation.

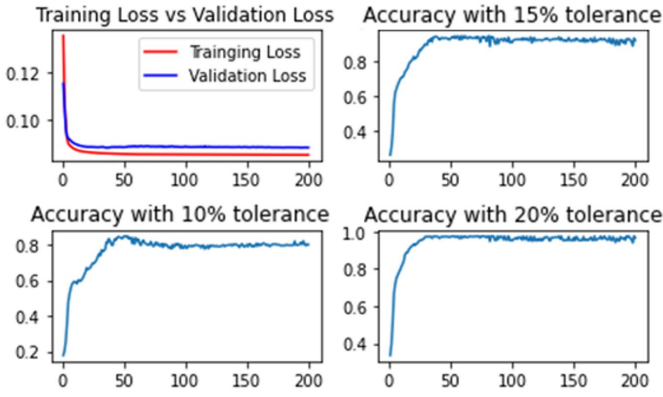


Fig. 7. Results of neural network training.

C. Results of NNODH algorithm

In this section, the BDMDS results obtained with the NNODH algorithm are presented. Table V presents the results for different strategies of the proposed NNODH algorithm presented in Section IV. The BCL, PBCL, BRL and ALL CMDS models are implemented and tested separately. The combination of all three types of constraints as the added constraints to MDS in the next iteration, marked as ALL in Table V, is tested as well. From Table V, we can observe that for all the proposed models, the maximum BDC is the same since the initial MDS formulation does not limit the battery operation. This also leads to the solution of the first iteration having the highest battery degradation cost. Similarly, the maximum total cost for different models is the same. For DCR, the BRL has the best performance among all the strategies. It can decrease the battery degradation cost by 39%. BRL also performs more efficient in terms of the decreased total cost. The performance on the increased operation cost is similar for BCL, BRL and All. Overall, we prefer the BRL due to its best performance to decrease the total cost and its least solving time.

Table V Results for proposed strategies

NNODH	BCL	PBCL	BRL	ALL
Maximum Degradation Cost	\$71.12	\$71.12	\$71.12	\$71.12
Maximum Total Cost	\$546	\$546	\$546	\$546
DCR	22.4%	10.8%	39%	36.82%
TCR	1.9%	0.86%	3%	2.88%
OCI	1.34%	3.84%	1.32%	1.52%
Solving time	65.28s	47.46s	46.92s	47.87s

Fig. 8 shows the results for NNODH-BRL including the degradation cost, operation cost, battery degradation in percent, and total cost. These results are based on the battery unit price of 200 \$/kWh and the value of BORF is set to be 0.03.

From Fig. 8, we can observe that the valley of the total cost curve is at the 28th iteration with \$529.52 including the equivalent battery degradation cost of \$43.33 and the microgrid operation cost of \$489.19. The total cost is reduced by 3% compared to the traditional MDS model that does not consider the battery degradation cost, which proves that the proposed NNODH algorithm can reduce the total cost significantly. Note that the results shown in Fig. 8 do not implement the stopping criteria to show how the system behaves when the battery's usage is further limited until idle. If not, the iteration will stop at the 33rd iteration. From the battery degradation curve, we can observe that the battery is substantially limited such that it stays idle after the 67th iteration. A non-zero degradation occurs when the battery is idle, which correspond to the battery calendar degradation. The total cost keeps constant when the BESS is in idle mode as is also shown in the total cost curve.

The scheduled BESS operation is shown in Fig. 9. Positive output means the BESS is in discharging mode and negative power means it is in charging mode. The scheduled BESS operations for both the traditional MDS model and the proposed BDMDS model are shown in Fig. 9. It can be observed for the traditional MDS without the consideration of battery degradation, the BESS operates at a wider output range from -150 kW to 150 kW in seven different time intervals. For the proposed BDMDS, after applying the NNODH algorithm to solve it, the BESS operates at a narrow range from -66 kW to 66 kW in nine different time intervals. The maximum output power and the total exchanged energy are limited to reduce the battery degradation which meets the designed objective of BRL.

Table VI shows the results of the sensitivity tests with different BORF values. The results show that larger BORF can achieve the lowest total cost in less iterations and less solving time. As a tradeoff, the optimal total cost of larger BORF will be slightly higher. This is because the larger BORF will cut off a bigger area of the feasible solution area in each iteration (shown in Fig. 6), which may lead to the best solution skipped from the global optimal solution. Smaller BORF will lead to a smaller area cut from the feasible solution area in each iteration, which requires more iterations to converge to the optimal solution. However, the optimal solutions for the different BORFs do not have a significant difference. Thus, a higher value of BORF such as 0.05 is preferred due to the high computing efficiency.

D. Sensitivity Analysis of BESS unit price and size

In this section, the sensitivity analysis on different BESS unit prices and sizes have been conducted. Table VIII and Fig. 10 shows that the total cost reduction in percentage. It can be clearly observed that for the same size of BESS, higher unit price corresponds to a higher total cost reduction in percent. For the same unit price of BESS, higher BESS size would result in a lower TCR. Table IX shows that for the same unit price, higher BESS size has a lower DCR. The reason is that for the same battery output power, bigger battery size will likely have a lower C rate that is one of the main contributing factors of battery degradation. Also, for the same size BESS, higher unit price results into a higher DCR but not significantly. Thus, we can conclude that the BESS price of per unit capacity is the major factor affecting how much the proposed

model reduces the degradation cost. The BESS size is the major factor affecting how much the proposed model reduces the battery degradation cost. The result of the sensitivity analysis in this section may help to determine the size of the BESS for the microgrid. In the meanwhile, the unit price of BESS keeps decreasing, so the battery degradation cost will be lower and account for smaller percentage respect to the total cost in the future.

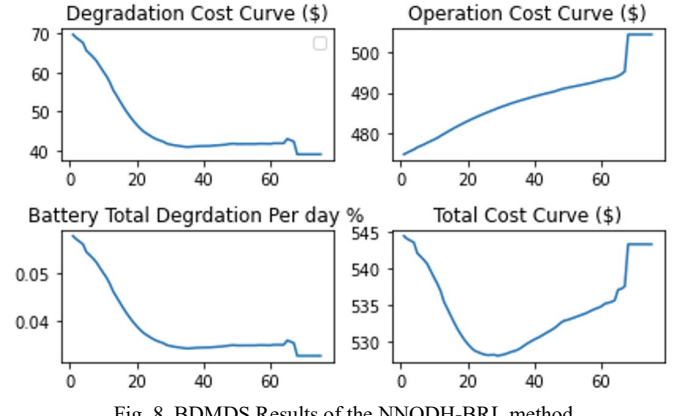


Fig. 8. BDMDS Results of the NNODH-BRL method.

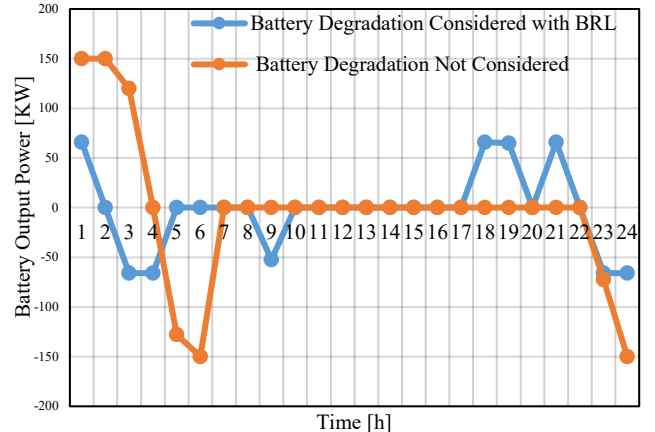


Fig. 9. BESS scheduled operations with and without battery degradation.

Table VI Results of sensitivity analysis with different BORF values

BORF	Number of Iterations	Optimal Total Cost (\$)	Time (s)
0.005	170	529.51	74.17
0.008	106	529.51	64.32
0.01	85	529.52	57.78
0.015	57	529.53	35.39
0.02	42	529.53	20.97
0.05	17	529.57	8.34

Table VII Results of different RES penetration levels

	RES Penetration Level			
	20%	40%	60%	80%
TCR	1.14%	1.38%	1.63%	2%
OCI	0.326%	0.40%	0.481%	0.6%

Table VIII TCR of different BESS sizes and unit prices

Size	TCR			
	80\$/kWh	120\$/kWh	150\$/kWh	200\$/kWh
200 kWh	0.99%	2.61%	3.83%	5.77%
300 kWh	0.56%	1.94%	3.03%	4.76%
400 kWh	0.32%	1.35%	2.21%	3.58%

Table IX DCR of different BESS sizes and unit prices

Size	DCR			
	80\$/kWh	120\$/kWh	150\$/kWh	200\$/kWh
200 kWh	59%	62%	63.1%	63.3%
300 kWh	44.2%	50.2%	50.6%	51.24%
400 kWh	33%	37.4%	37.4%	38.41%

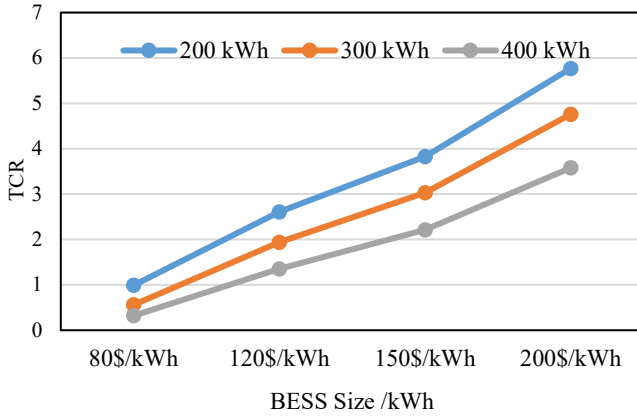


Fig. 10. BESS scheduled operation.

VI. CONCLUSIONS

In this paper, a neural network based battery degradation model is proposed to predict the BESS degradation value for each scheduling period. The NNODH algorithm is proposed to decouple the BDMDS problem that is hard to solve directly due to the highly non-linear characteristic of the proposed NNBD model. The proposed NNODH algorithm can solve the MDS optimization problem, calculate the battery degradation cost and find the optimal solution with the lowest total cost. Three different types of constraints, BCL, PBCL, and BRL are proposed to be added in the CMDS problem separately to limit the BESS usage to obtain a lower cost of battery degradation. An RES-enriched microgrid is used to evaluate the performance of the proposed BDMDS model and the proposed NNODH algorithm.

The test results demonstrate that the battery degradation can be accurately predicted by the proposed NNBD model. The proposed NNODH algorithm can obtain the optimal solution efficiently. The total cost can be reduced significantly with the proposed BDMDS model comparing to the traditional MDS model. The NNODH-BRL is proved to be the best performance strategy among the proposed four NNODH strategies. Sensitivity tests demonstrate the performance of the proposed NNODH algorithm under different BESS sizes and unit prices. Overall, this work demonstrates the effectiveness of the proposed BDMDS model for reducing battery degradation cost and total cost, and the capability of the proposed NNODH algorithm for efficiently solving BDMDS that is a deep neural network embedded optimization problem.

REFERENCES

- B. Li, T. Chen, X. Wang and G. Giannakis, "Real-Time Energy Management in Microgrids With Reduced Battery Capacity Requirements," *IEEE Trans. Smart Grid.*, vol. 10, no. 2, pp. 1928–1938, Mar. 2019.
- M. T. Lawder et al., "Battery Energy Storage System (BESS) and Battery Management System (BMS) for Grid-Scale Applications," in *Proceedings of the IEEE*, vol. 102, no. 6, pp. 1014-1030, June 2014.
- X. Gong, R. Xiong and C. C. Mi, "Study of the Characteristics of Battery Packs in Electric Vehicles With Parallel-Connected Lithium-Ion Cells," in *IEEE Transactions on Industry Applications*, vol. 51, no. 2, pp. 1872-1879, March-April 2015.
- Z. Lyu, R. Gao, and L. Chen, "Li-ion Battery State of Health Estimation and Remaining Useful Life Prediction Through a Model-Data-Fusion Method," *IEEE TRANSACTIONS ON POWER ELECTRONICS*, vol. 36, no. 6, pp. 6228–6240, June. 2021.
- B. Xu, A. Oudalov, A. Ulbig, G. Andersson and D. Kirschen, "Modeling of lithium-ion battery degradation for cell life assessment," *2017 IEEE Power & Energy Society General Meeting*, 2017, pp. 1-1.
- P. S. Kumar, R. P. S. Chandrasena, V. Ramu, G. N. Srinivas and K. V. S. M. Babu, "Energy Management System for Small Scale Hybrid Wind Solar Battery Based Microgrid," in *IEEE Access*, vol. 8, pp. 8336-8345, 2020.
- A. Merabet, K. Tawfique Ahmed, H. Ibrahim, R. Beguenane and A. M. Y. M. Ghias, "Energy Management and Control System for Laboratory Scale Microgrid Based Wind-PV-Battery," in *IEEE Transactions on Sustainable Energy*, vol. 8, no. 1, pp. 145-154, Jan. 2017.
- X. Xing, L. Xie, H. Meng, X. Guo, L. Yue and J. M. Guerrero, "Energy management strategy considering multi-time-scale operational modes of batteries for the grid-connected microgrids community," in *CSEE Journal of Power and Energy Systems*, vol. 6, no. 1, pp. 111-121, March 2020.
- K. Thirugnanam, S. K. Kerk, C. Yuen, N. Liu and M. Zhang, "Energy Management for Renewable Microgrid in Reducing Diesel Generators Usage With Multiple Types of Battery," in *IEEE Transactions on Industrial Electronics*, vol. 65, no. 8, pp. 6772-6786, Aug. 2018.
- Z. Miao, L. Xu, V. R. Disfani and L. Fan, "An SOC-Based Battery Management System for Microgrids," in *IEEE Transactions on Smart Grid*, vol. 5, no. 2, pp. 966-973, March 2014.
- B. Li, T. Chen, X. Wang and G. B. Giannakis, "Real-Time Energy Management in Microgrids With Reduced Battery Capacity Requirements," in *IEEE Transactions on Smart Grid*, vol. 10, no. 2, pp. 1928-1938, March 2019.
- C. Zhao and X. Li, "A Novel Real-Time Energy Management Strategy for Grid-Friendly Microgrid: Harnessing Internal Fluctuation Internally", *52nd North American Power Symposium*, (Virtually), Tempe, AZ, USA Apr. 2021.
- C. Zhao and X. Li, "A Novel Real-Time Energy Management Strategy for Grid-Supporting Microgrid: Enabling Flexible Trading Power", *IEEE PES General Meeting*, (Virtually), Washington D.C., USA, Jul. 2021.
- C. Ju, P. Wang, L. Goel and Y. Xu, "A Two-Layer Energy Management System for Microgrids With Hybrid Energy Storage Considering Degradation Costs," in *IEEE Transactions on Smart Grid*, vol. 9, no. 6, pp. 6047-6057, Nov. 2018.
- L. De Pascali, F. Biral and S. Onori, "Aging-Aware Optimal Energy Management Control for a Parallel Hybrid Vehicle Based on Electrochemical-Degradation Dynamics," in *IEEE Transactions on Vehicular Technology*, vol. 69, no. 10, pp. 10868-10878, Oct. 2020.
- J. Cao, D. Harrold, Z. Fan, T. Morstyn, D. Healey and K. Li, "Deep Reinforcement Learning-Based Energy Storage Arbitrage With Accurate Lithium-Ion Battery Degradation Model," in *IEEE Transactions on Smart Grid*, vol. 11, no. 5, pp. 4513-4521, Sept. 2020.
- G. Abdelaal, M. I. Gilany, M. Elshahed, H. M. Sharaf and A. El'gharably, "Integration of Electric Vehicles in Home Energy Management Considering Urgent Charging and Battery Degradation," in *IEEE Access*, vol. 9, pp. 47713-47730, 2021.
- K. Abdulla et al., "Optimal operation of energy storage systems considering forecasts and battery degradation," *2017 IEEE Power & Energy Society General Meeting*, 2017, pp. 1-1.
- K. Antoniadou-Plytaria, D. Steen, L. A. Tuan, O. Carlson and M. A. Fotouhi Ghazvini, "Market-Based Energy Management Model of a Building Microgrid Considering Battery Degradation," in *IEEE Transactions on Smart Grid*, vol. 12, no. 2, pp. 1794-1804, March 2021.
- G. Saldaña, J. I. S. Martín, I. Zamora, F. J. Asensio, O. Oñederra and M. González, "Empirical Electrical and Degradation Model for Electric Vehicle Batteries," in *IEEE Access*, vol. 8, pp. 155576-155589, 2020.
- Y. Sun, H. Yue, J. Zhang and C. Booth, "Minimization of Residential Energy Cost Considering Energy Storage System and EV With Driving Usage Probabilities," in *IEEE Transactions on Sustainable Energy*, vol. 10, no. 4, pp. 1752-1763, Oct. 2019.
- H. Farzin, M. Fotouhi-Firuzabad and M. Moeini-Aghajaei, "A Practical Scheme to Involve Degradation Cost of Lithium-Ion Batteries in Ve-

hicle-to-Grid Applications," in *IEEE Transactions on Sustainable Energy*, vol. 7, no. 4, pp. 1730-1738, Oct. 2016.

[23] Z. Wei, Y. Li and L. Cai, "Electric Vehicle Charging Scheme for a Park-and-Charge System Considering Battery Degradation Costs," in *IEEE Transactions on Intelligent Vehicles*, vol. 3, no. 3, pp. 361-373, Sept. 2018.

[24] S. Fang, B. Gou, Y. Wang, Y. Xu, C. Shang and H. Wang, "Optimal Hierarchical Management of Shipboard Multibattery Energy Storage System Using a Data-Driven Degradation Model," in *IEEE Transactions on Transportation Electrification*, vol. 5, no. 4, pp. 1306-1318, Dec. 2019.

[25] Omar N., M. A. Monem, Y. Firouz, J. Salminen, J. Smekens, O. Hegazy, H. Gaulous, G. Mulder, P. Van den Bossche, T. Coosemans, and J. Van Mierlo. "Lithium iron phosphate based battery — Assessment of the aging parameters and development of cycle life model." *Applied Energy*, Vol. 113, January 2014, pp. 1575–1585.

[26] S. Saxena, C. Floth, J. MacDonald, S. Moura, "Quantifying EV battery end-of-life through analysis of travel needs with vehicle powertrain models," in *Journal of Power Sources*, vol. 282, pp. 265-276, Jan. 2015.

[27] S. Loffe, C.Szegedy, "Batch Normalization: Accelerating Deep Network Training by Reducing Internal Covariate Shift," in *Proceedings of the 32nd International Conference on Machine Learning*, Vol. 37,pp. 448-456, Mar. 2015.

[28] NN-SVG, <http://alexlenail.me/NN-SVG/index.html>.

[29] "Dataport Resources," May, 2019 [online] Available: <https://dataport.pecanstreet.org/academic>.

[30] "ERCOT, Electric Reliability Council of Texas," [Online]. Available: <http://www.ercot.com/>.

[31] "Pyomo, Python Software packages.," Available: [Online]. Available: <http://www.pyomo.org/>.

[32] "Gurobi Optimization, Linear Programming Solver," [Online]. Available: <https://www.gurobi.com/>.